

NASA Technical Paper 1257

LOAN COPY: RET
AFWL TECHNICAL
KIRTLAND AFB,

0134352



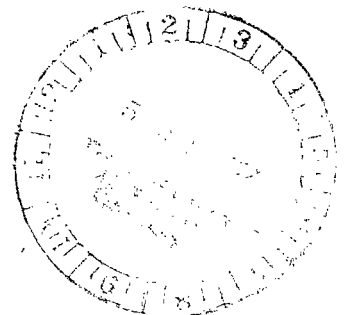
TECH LIBRARY KAFB, NM

Fluctuation Spectra in the NASA Lewis Bumpy-Torus Plasma

Chandra M. Singh, Walter M. Krawczonek,
J. Reece Roth, Jae Y. Hong, and Edward J. Powers

JUNE 1978

NASA





NASA Technical Paper 1257

Fluctuation Spectra in the NASA Lewis Bumpy-Torus Plasma

Chandra M. Singh, Walter M. Krawczonek,
and J. Reece Roth
*Lewis Research Center
Cleveland, Ohio*

Jae Y. Hong and Edward J. Powers
*University of Texas
Austin, Texas*

NASA

National Aeronautics
and Space Administration

**Scientific and Technical
Information Office**

1978

CONTENTS

	Page
SUMMARY	1
INTRODUCTION	1
FLUCTUATION DIAGNOSTICS	3
Data Acquisition	3
Data Processing and Analysis	5
System Calibration	8
RESULTS	10
High-Pressure (Low Impedance) Mode	10
Low-Pressure (High Impedance) Mode	16
DISCUSSION	21
CONCLUSIONS	23
APPENDIX - SYMBOLS	24
REFERENCES	26

FLUCTUATION SPECTRA IN THE NASA LEWIS BUMPY-TORUS PLASMA

by Chandra M. Singh,* Walter M. Krawczonek, J. Reece Roth,
Jae Y. Hong,** and Edward J. Powers†

Lewis Research Center

SUMMARY

The electrostatic potential fluctuation spectrum in the NASA Lewis bumpy-torus plasma was studied with capacitive probes in the low-pressure (high impedance) mode and the high-pressure (low impedance) mode. Under different operating conditions, the plasma exhibited electrostatic potential fluctuations (1) at a set of discrete frequencies, (2) at a continuum of frequencies, and (3) as incoherent high-frequency turbulence. The frequencies and azimuthal wave numbers were determined from digitally implemented autopower and cross-power spectra. The azimuthal dispersion characteristics of the unstable waves were examined by varying the electrode voltage, the polarity of the voltage, and the neutral background density at a constant magnetic field strength.

INTRODUCTION

The NASA Lewis bumpy-torus plasma is produced, heated, and confined by a combination of strong, crossed electric and magnetic fields. The bumpy-torus magnetic field is generated by an array of 12 superconducting coils equally spaced around the major axis of a torus of 1.52-meter major diameter. A circular electrode ring can be installed around the minor circumference of the plasma at the midplane of each of the 12 sectors. The electrodes can be biased with positive or negative polarity with respect to the grounded magnet dewars. The magnetic axis is displaced from the geometric axis toward the inside of the torus by 6.1 centimeters. In this experiment, the plasma, the electrode potentials, and the confining magnetic field were operated in the steady state.

* National Research Council - National Aeronautics and Space Administration
Research Associate.

** University of Texas, Austin, Texas.

† Professor of Electrical Engineering, University of Texas, Austin, Texas.

pearing as fluctuations and the fraction serving as a direct-current (dc) bias of the toroidal plasma ring for a given dc potential applied to the electrode ring.

The preliminary results reported herein were obtained in a deuterium plasma. The maximum magnetic field B_{\max} on a coil axis was kept constant at 2.4 teslas. Since the magnetic field decreases with major radius R , the lowest magnetic field at the midplane of a sector was not at the geometric axis ($R = 0.76$ m) but at a radius of $R + r_A$, where r_A is the radius of the electrode ring. The electrode rings used in the present investigation had an inside diameter of 18 centimeters and were installed concentric with the geometric axis. The minimum field for an r_A of 9 centimeters was 0.47 tesla. The direction of the magnetic field was clockwise, viewed from the top of the facility in figure 1. The 12 sectors of the toroidal array are spaced 30° apart and are numbered in the counterclockwise direction, viewed from the top of the facility. The capacitive probe assembly was located near the midplane of sector 4; the microwave interferometer, in sector 10; and the neutral particle energy analyzer, in sector 9.

Clay Boyd of the University of Texas helped design the data-processing system and Y.C. Kim, also of the University of Texas, processed the data.

FLUCTUATION DIAGNOSTICS

Data Acquisition

A block diagram of the data-acquisition system is shown in figure 2. The potential fluctuations were measured by capacitive probes. The gain and frequency response of each probe were measured on a test bench. The frequency response was flat from 1 kilohertz to 5 megahertz - the frequency range of interest. From the gain of the probe system, the absolute amplitude of the potential fluctuations in the plasma was determined.

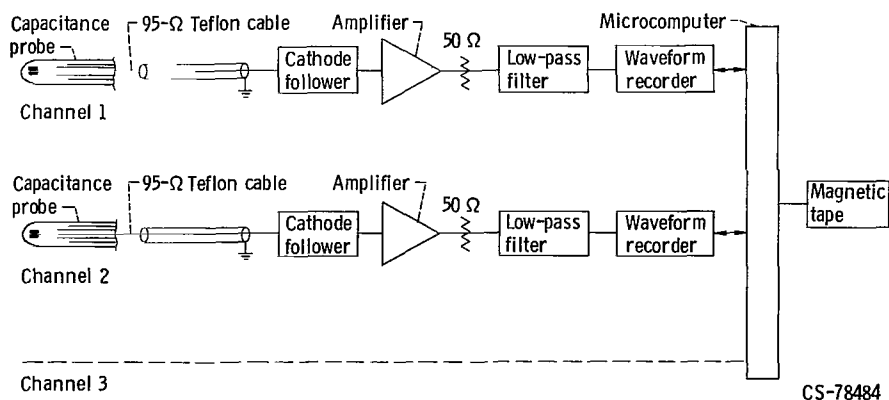
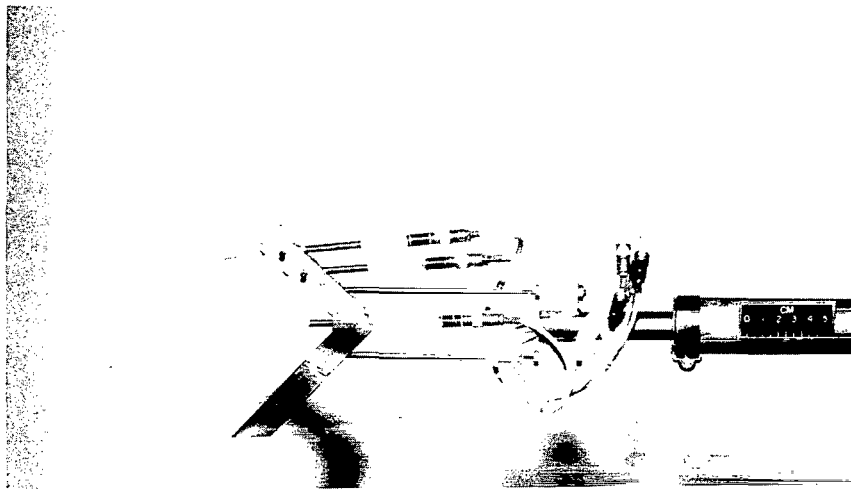
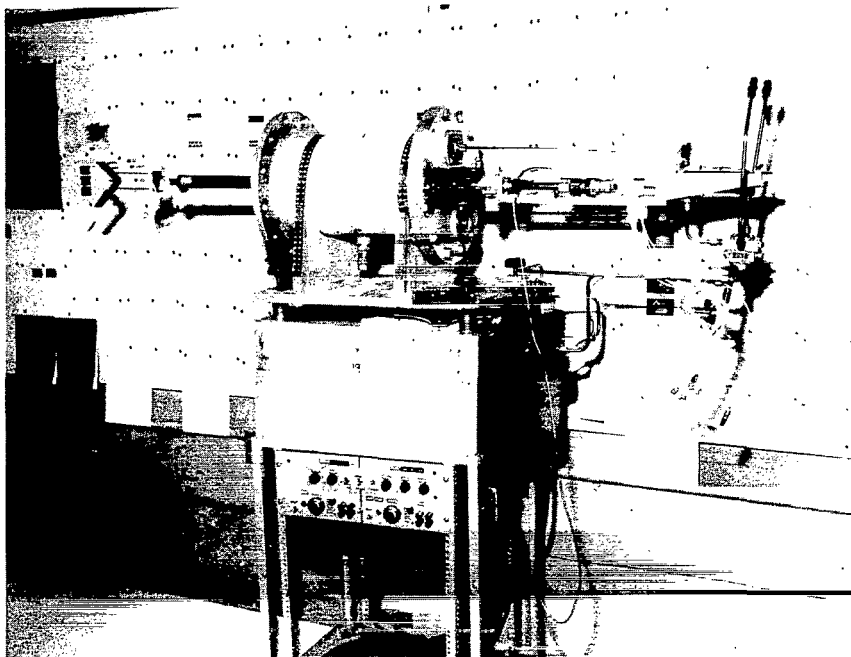


Figure 2. - Block diagram of data-acquisition system.

The capacitive probes were hydraulically actuated into the plasma for short times to take data. This procedure was necessary because otherwise the probes would glow red hot and the probability of arcing to the probe assembly would be high. The dwell time of the probes in the plasma could be adjusted between 0.1 and 0.7 second. For these data, the dwell time was 0.7 second, and the data were sampled 0.3 second into the dwell time. Figure 3(a) is a closeup view of three capacitive probes in the probe mount. Figure 3(b) shows the entire probe assembly. The metallic probe mount always stayed out-



(a) Closeup view of capacitive probes.



(b) Entire assembly and actuation system.

Figure 3. - Probe assembly.

side the plasma. The gross plasma characteristics, such as number density and electrode current, were not significantly perturbed when the probes were inserted into the plasma. The length of probe travel was adjusted so that, at a plasma radius of 7 centimeters, if the first probe was in the equatorial plane, the second probe was 30° above it, and the third probe was 45° above the first. This probe arrangement yields information on the azimuthal wave number k_θ only.

A low-pass filter was connected before the waveform recorder, in some cases, to avoid aliasing. For a detailed discussion on aliasing, see references 8 and 9. The waveform recorder digitizes the analog fluctuation signal and stores it in its memory. The digitized signal from the memory can be stored on a magnetic tape or displayed on an oscilloscope after digital-to-analog conversion. For the present investigation, only two capacitive probes separated in azimuth by 30° were used to record data on two waveform recorders. A typical run consisted of actuating the probes into the plasma; recording the data on the waveform recorders, starting 0.3 second after actuation; bringing the probes out of the plasma 0.7 second after actuation; and finally recording the data on the magnetic tape from the waveform recorders. The data length was in all cases much less than the dwell time of the probe in the plasma.

Data Processing and Analysis

After the data had been stored on a magnetic tape at NASA Lewis, the tape was sent to the University of Texas at Austin for processing on their CDC 6600 computer. Figure 4 is a schematic of the data-processing system. The computer output yields the statistical functions of interest. Space-time statistics yield information on the frequency, wave number, and amplitude of the fluctuations in the data. The space-time statistical

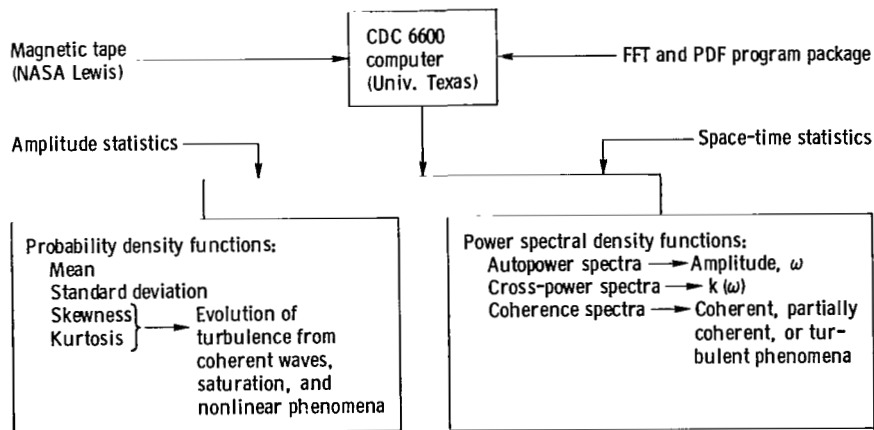


Figure 4. - Schematic of data-processing system.

functions used in this study are defined explicitly as follows (where symbols are defined in the appendix): The amplitude of the electrostatic potential at position \mathbf{r} and time t is the integral over all frequencies of its Fourier spectral components.

$$\varphi(\bar{\mathbf{r}}, t) = \int_{-\infty}^{\infty} \varphi_0(\omega) e^{i[\bar{\mathbf{k}}(\omega) \cdot \bar{\mathbf{r}} - \omega t]} d\omega \quad (1)$$

The potential at probe 1 is

$$\varphi_1(t) \equiv \varphi(\bar{\mathbf{r}}_1, t) \quad (2a)$$

and that at probe 2 is

$$\varphi_2(t) \equiv \varphi(\bar{\mathbf{r}}_2, t) \quad (2b)$$

The Fourier transforms of the potentials at these two probes are

$$\varphi_1(\omega) = \varphi_0(\omega) e^{i\bar{\mathbf{k}}(\omega) \cdot \bar{\mathbf{r}}_1} \quad (3a)$$

and

$$\varphi_2(\omega) = \varphi_0(\omega) e^{i\bar{\mathbf{k}}(\omega) \cdot \bar{\mathbf{r}}_2} \quad (3b)$$

The autopower spectra of the potentials at the two probes can be written in terms of the Fourier transform of the amplitude and its complex conjugate or in terms of the square of the absolute magnitude of the Fourier transform:

$$P_{11}(\omega) = \varphi_1(\omega) \varphi_1^*(\omega) = |\varphi_0(\omega)|^2 \quad (4a)$$

and

$$P_{22}(\omega) = \varphi_2(\omega) \varphi_2^*(\omega) = |\varphi_0(\omega)|^2 \quad (4b)$$

The cross-power spectrum of the two probes can be written

$$P_{12}(\omega) = \varphi_1(\omega) \varphi_2^*(\omega) = |\varphi_0(\omega)|^2 e^{i\bar{\mathbf{k}}(\omega) \cdot \Delta \bar{\mathbf{r}}} \quad (5)$$

where the square of its absolute magnitude is

$$|P_{12}(\omega)| = |\varphi_0(\omega)|^2 \quad (6)$$

and the phase angle between the two signals at the frequency is

$$\theta_{12}(\omega) = \bar{k}(\omega) \cdot \Delta\bar{r} \quad (7)$$

The coherence spectrum is defined as

$$|\gamma_{12}(\omega)| = \frac{|P_{12}(\omega)|}{[P_{11}(\omega)P_{22}(\omega)]^{1/2}} \quad (8)$$

For more detailed definitions of the statistical functions, see references 9 and 10.

The preceding definitions include the following assumptions, which define a plasma model that is discussed more fully in reference 11:

(1) The autopower spectral density functions are identical at each point; that is

$$P_{11}(\omega) = P_{22}(\omega) = |\varphi_0(\omega)|^2 \quad (9)$$

(2) The coherence is unity; that is, $|\gamma_{12}(\omega)| = 1$.

(3) The cross-power spectrum is equal to the autopower spectrum; that is,

$$P_{12}(\omega) = P_{11}(\omega) = P_{22}(\omega) = |\varphi_0(\omega)|^2 \quad (10)$$

(4) The phase spectrum is a direct measure of the dispersive characteristics of the system; that is,

$$\theta_{12}(\omega) = \bar{k}(\omega) \cdot \Delta\bar{r} \quad (11a)$$

where

$$\Delta\bar{r} = \bar{r}_1 - \bar{r}_2 \quad (11b)$$

The model also assumes that a wave is not damped as it propagates from one point to another. In addition, the effects of background noise are not included. The presence of noise or the frequency averaging described in reference 11 result in a coherence of less than unity. This effect is discussed in detail in reference 12.

The azimuthal phase velocity in a cylindrical geometry can be evaluated from the phase difference between the two probes $\theta_{12}(\omega)$, obtained from a plot of the phase spectrum, and from the azimuthal probe separation $\Delta\theta$. The wave-number spectrum can be written

$$k_{\theta}(\omega) = \frac{\theta_{12}(\omega)}{r \Delta\theta} \quad (12)$$

and the phase velocity is just

$$v_{\text{ph}\theta} = \frac{\omega}{k_{\theta}} = \frac{\omega r \Delta\theta}{\theta_{12}(\omega)} \quad (13)$$

Recapitulating, coherent wave phenomena in some spectral bands can be identified by observing the peaks in the autopower spectra $P_{11}(\omega)$ and $P_{22}(\omega)$ and the cross-power spectrum $|P_{12}(\omega)|$. If the coherence spectrum in the same spectral bands is reasonably high, this model can be used with confidence. There is also less jitter in those spectral bands of the phase where there are peaks in autopower and cross-power spectra and high coherence.

System Calibration

Before the plasma data were processed and analyzed, the data-acquisition system was checked by known test signals. Test waveforms of known amplitude, frequency, and waveshape were applied to the input of the waveform recorders. Figure 5 shows the computer output generated by applying the same 50-kilohertz square test waveform across the inputs of the two waveform recorders. The advantage of a square test waveform is that, by choosing a proper sampling interval, one should be able to follow up to the ninth harmonic of the fundamental frequency in the square waveform. The relative strength of the harmonics generated by the computer plots of autopower spectra can also be compared with the analytically calculated values. From figure 5,

(1) The autopower spectrum and the cross-power spectrum have peaks at 50, 150, 250, 350, and 450 kilohertz.

(2) The relative amplitudes of the peaks in the computer-generated autopower spectra agree quite closely with the analytical values. The autopower spectrum plot of channel 1 in figure 5 shows the computer-generated values in parentheses and the analytical values outside parentheses. Their similarity instills confidence in the computer software used to generate the power spectra.

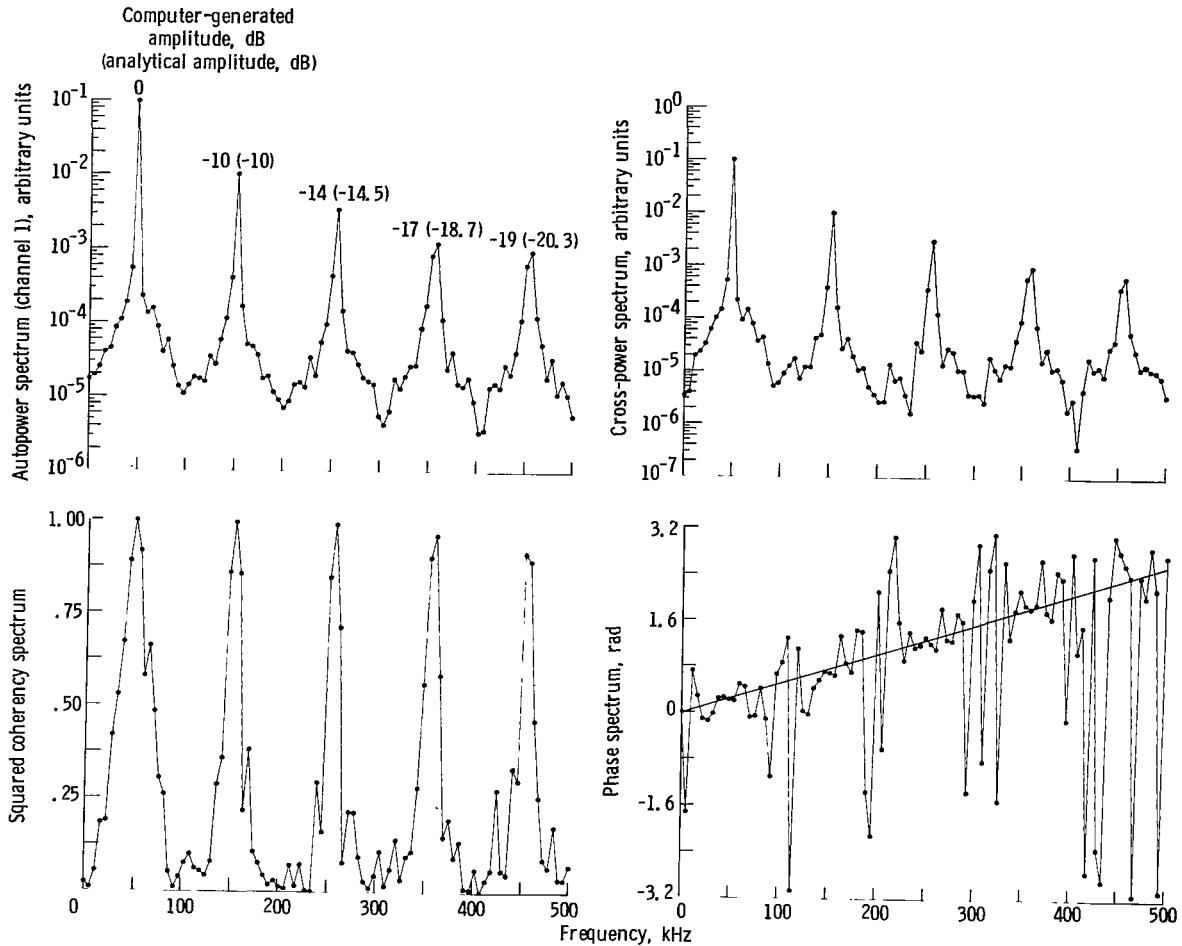


Figure 5. - Test data for 50-kilohertz square wave. Sampling interval, Δt , 1 μ sec.

(3) The squared coherency spectrum has rather high values (>0.87) in the spectral bands corresponding to the peaks in the autopower spectrum.

(4) The phase spectrum has almost no jitter in the spectral bands corresponding to the peaks in the power spectra. However, in those bands where there are no peaks in the power spectra and the squared coherency spectrum has values less than 0.25, the phase spectrum is random and jittery. This is characteristic of noise.

Since the same 50-kilohertz square waveform was applied across the inputs of the two waveform recorders, there should be a phase difference of zero radians at the frequencies corresponding to the peaks in the power spectra if there is no time delay in the system. It was concluded after power spectra had been generated for different waveforms, frequencies, and sampling intervals that there was a constant time delay at all the frequencies, as shown in figure 5. This instrumentation time delay depended only on the sampling interval. All subsequent plasma data were therefore corrected accordingly.

The computer output plots show the squared coherency spectrum rather than the coherency spectrum. A high value of the squared coherency spectrum is a more stringent criterion than a high value of the coherence spectrum.

RESULTS

The bumpy-torus plasma operates in two modes: the high-pressure mode, and the low-pressure mode. In the literature, the high-pressure mode is sometimes also called the low-impedance mode, and the low-pressure mode is also called the high-impedance mode.

High-Pressure (Low Impedance) Mode

In deuterium, operation of the bumpy torus in the high-pressure mode (HPM) is characterized by an electron kinetic temperature T_e of $\lesssim 35$ electron volts and a neutral background density n_0 of $\geq 8.9 \times 10^{11}$ particles per cubic centimeter ($\gtrsim 2.7 \times 10^{-5}$ torr, ref. 4). All the data presented herein were taken with an n_0 of 1.8×10^{12} particles per cubic centimeter (5.3×10^{-5} torr).

Figure 6 presents the cross-power spectrum, the phase spectrum, and the squared coherency spectrum with the electrodes in sectors 5 and 6 surrounding the plasma. All other electrodes were withdrawn from the experimental volume. The electrodes were biased to a potential of 2 kilovolts. The cross-power spectrum has peaks at 220, 440, 616, and 880 kilohertz. The squared coherency spectrum has high values corresponding to these frequencies. The frequencies are harmonically related. For the fundamental and second harmonics the coherency γ_{12} is greater than 0.87. The peak corresponding to the third harmonic is shifted down on the frequency scale by 44 kilohertz, which is within the frequency resolution for this plot. Values of $|\gamma_{12}|$ are not expected to be as high for the third and fourth harmonics as for the first two harmonics because the difference in power levels is greater than 10 decibels. The power level of the fourth harmonic is barely above the noise level. For those spectral bands in the cross-power spectrum where the peaks occur, the phase spectrum is quiet and has very little jitter. The phase corresponding to the peaks is linearly related to the frequencies of the peaks in the cross-power spectrum. This can be seen by drawing a straight line from the origin through the points in the phase spectrum that correspond to the peaks in the cross-power spectrum. The slope of this line, after a correction for the instrumentation time delay, yields a phase velocity of 7.3×10^6 centimeters per second.

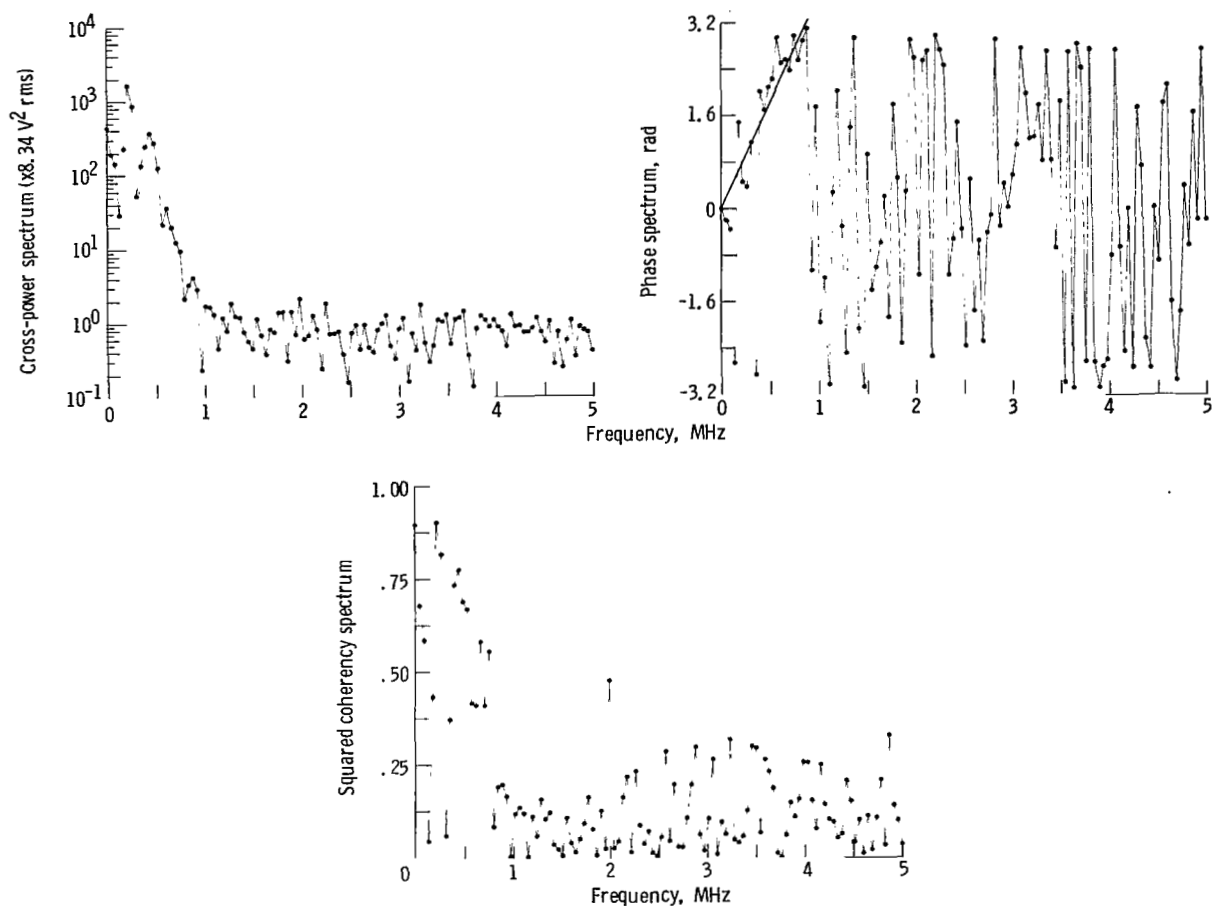


Figure 6. - Wave dispersion with electrodes 5 and 6 in plasma and 2-kilovolt anode voltage. Mode of operation, high pressure; sampling interval, Δt , 0.1 microsecond.

When a positive polarity is applied to the electrode rings, the electric field near the anode rings points radially inward into the plasma. At all other points, the electric field points radially outward. The periphery of the plasma is subjected to two oppositely directed E/B drift velocities. The direction of wave propagation can be compared with the E/B drift direction and is determined by comparing the phase at the two probe locations. For the experimental run shown in figure 6 the wave was traveling in the direction of the E/B drift, with the electric field pointing radially outward. The absolute value of the E/B drift velocity can also be compared with the experimentally measured, azimuthal, phase velocity. The radial electric field was not measured in the present investigation. However, E/B drift velocity can be estimated by noting that, if a disturbance is propagating around a circular (or other closed) path, an upper limit to the wavelength of the permissible disturbances is given by the perimeter of the path. The circumference at the radial location of the probes is 44 centimeters. The time in which a disturbance propagates around this circumference is the time period of the wave cor-

responding to 220 kilohertz. The estimated E/B drift velocity is then 9.6×10^6 centimeters per second, which agrees with the measured, azimuthal, wave-phase velocity within the limits of experimental error. This drift velocity corresponds to an equivalent radial electric field of 400 volts per centimeter. A reader interested in azimuthal mode numbers can observe from figure 6 and the preceding discussion that the mode numbers are

Mode, m	Frequency, ω , kHz
1	220
2	440
3	616
4	880

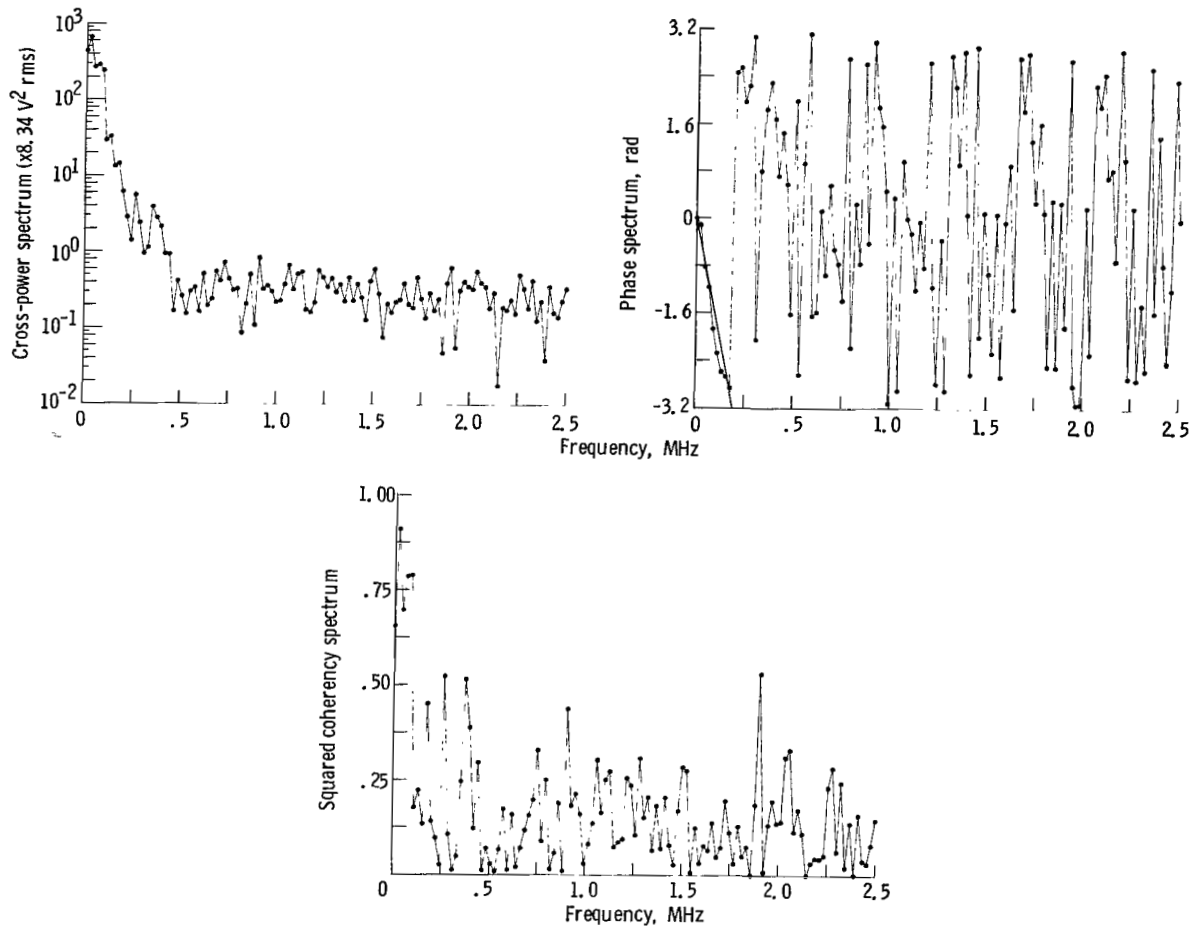


Figure 7. - Wave dispersion with electrodes 5 and 6 in plasma and -2-kilovolt electrode voltage. Mode of operation, high pressure; sampling interval, Δt , 0.2 microsecond.

This is a case of resonant harmonic generation, in that the resonance conditions on both ω and k_θ (or m) are satisfied. The resonance conditions are

$$\omega_1 + \omega_2 = \omega_3 \quad (14)$$

and

$$k_1 + k_2 = k_3 \quad (15)$$

One final observation from figure 6 is that the spectral band from 1 to 5 megahertz has no peaks, very low coherency, and a random and jittery phase - characteristics of noise.

Figure 7 presents the wave dispersion relation when the electrodes in sectors 5 and 6 were biased to a potential of -2 kilovolts. The peaks in the cross-power spectra that have a high coherency are at 88, 176, 264, and 352 kilohertz. The frequencies are harmonically related, and up to the fourth harmonic of the fundamental is present in the plasma. Again a straight line can be drawn through the origin and the phase points corresponding to frequencies of 88 and 176 kilohertz in the phase spectrum plot. The points corresponding to 264 and 352 kilohertz do not lie on this straight line because the computer only determines the principal value of the phase spectrum (i. e. , all values lie within $-\pi \leq \theta_{12}(\omega) \leq +\pi$. The true value of $\theta_{12}(\omega)$ may differ from the principal value by $\pm n2\pi$ radians, where $n = 0, 1, 2, \dots$. In cylindrical coordinates, the addition of 2π relates to an inability to distinguish experimentally between, for example, an $m = 1$ and an $m = 13$ wave in the plasma. That is,

$$m(\omega) = \frac{\theta_{12}(\omega) \pm n2\pi}{\Delta\theta} = \frac{\theta_{12}(\omega)}{\Delta\theta} \pm 12n \quad (16)$$

where, for this facility, $\Delta\theta = \pi/6$ radians. Subtracting 2π from the phase spectrum at 264 and 352 kilohertz puts them very close to the straight line drawn through the origin and the first two harmonic points. This suggests that the phase velocity of all the harmonics is the same. After a correction for instrumentation time delay, figure 7 yields a measured azimuthal phase velocity of -1.3×10^6 centimeters per second that is in the same direction as the E/B drift velocity, with the electric field pointing radially inward. Note that the resonance conditions on both ω and k_θ are satisfied in this case.

In figure 6, for a maximum magnetic field B_{\max} of 2.4 teslas and a neutral background density n_0 of 1.8×10^{12} particles per cubic centimeter (5.3×10^{-5} torr) and with a positive potential of 2 kilovolts on electrode rings 5 and 6, positive phase shift implied that the wave is propagating in the same direction as the E/B drift. Similar results are shown in figure 7 for conditions in which only the polarity of the applied potential on the

electrode rings is changed from that of figure 6. This change of polarity, and thus of the direction of the E/B drift, causes a change in direction of the phase shift between probes. Thus, for these two cases of opposite polarities, the azimuthal phase velocities are in the same direction as the E/B drift velocity.

TABLE I. - EFFECTS OF CHANGING POLARITY AND LOCATION OF TWO ELECTRODE RINGS IN HIGH-PRESSURE MODE OF OPERATION

Parameter	Electrodes 1 and 7	Electrodes 5 and 6	
	Anode voltage, V_a , kV		
	2	2	-2
Electron density, n_e , electrons/cm ³	7.2×10^9	1.2×10^{10}	6.5×10^9
Frequency, ω , kHz	220, 352, 440, 528	220, 440, 616, 880	88, 176, 264, 352
Amplitude phase velocity, $v_{ph\theta}$, cm/sec	^a 1.3×10^7 ^b -2.7×10^6	7.3×10^6	-1.3×10^6

^aAt 220 and 440 kHz.

^bAt 352 and 528 kHz.

Table I shows in more detail the effects of changing the relative location of the electrode rings and the polarity of the applied potential. All the cases in table I have the same magnetic field, the same magnitude of applied voltage, the same pressure, and the same polarity applied to each of two electrode rings. With electrodes 5 and 6 installed, changing the polarity changes the plasma density and the frequencies that are excited in the plasma. However, the direction of the azimuthal phase velocities is the same as the direction of the E/B drift velocity. For both polarities, four modes are generated in the plasma and all four travel with the same phase velocity.

However, comparing the case having electrodes 1 and 7 biased to 2 kilovolts with the case having electrodes 5 and 6 biased to 2 kilovolts shows that, in addition to a change in the plasma density, the wave phenomena have changed radically. With electrodes 1 and 7 the wave modes at 220 and 440 kilohertz are harmonically related in frequency and travel with the same phase velocity (1.3×10^7 cm/sec) in the direction of the E/B drift velocity with the electric field pointing radially outward. The wave modes at 352 and 528 kilohertz appear to be the sidebands of the mode at 440 kilohertz, with the sum and difference frequency of 88 kilohertz. The sidebands travel with an azimuthal phase velocity of -2.7×10^6 centimeters per second. The direction of their travel corresponds to the direction of the E/B drift velocity that is driven by the electric field between the anode ring and the plasma. However, the direction of mode propagation at 220 and 440 kil-

ohertz corresponds to the direction of the drift velocity that is driven by the electric field between the plasma and the grounded dewars.

The question that may be asked is whether the plots have simply failed to show a peak at 88 kilohertz or the wave mode at 88 kilohertz is buried in the noise. Examining the 88-kilohertz phenomenon may depend on improving the frequency resolution of the computer plots.

To explore the sideband phenomena - the direction of sideband propagation and the presence or absence of a mode at 88 kilohertz - we increased the positive bias on electrode rings 1 and 7 from 2 kilovolts to 4 kilovolts but kept the magnetic field and the neutral particle density the same. The computer plots are presented in figure 8. The cross-power spectrum has peaks at 88 and 176 kilohertz; 352, 440, and 572 kilohertz; and 792, 880, and 1012 kilohertz. The peaks at 88 and 176 kilohertz are harmonically related in frequency and propagate with the same azimuthal velocity of -5.1×10^6 centi-

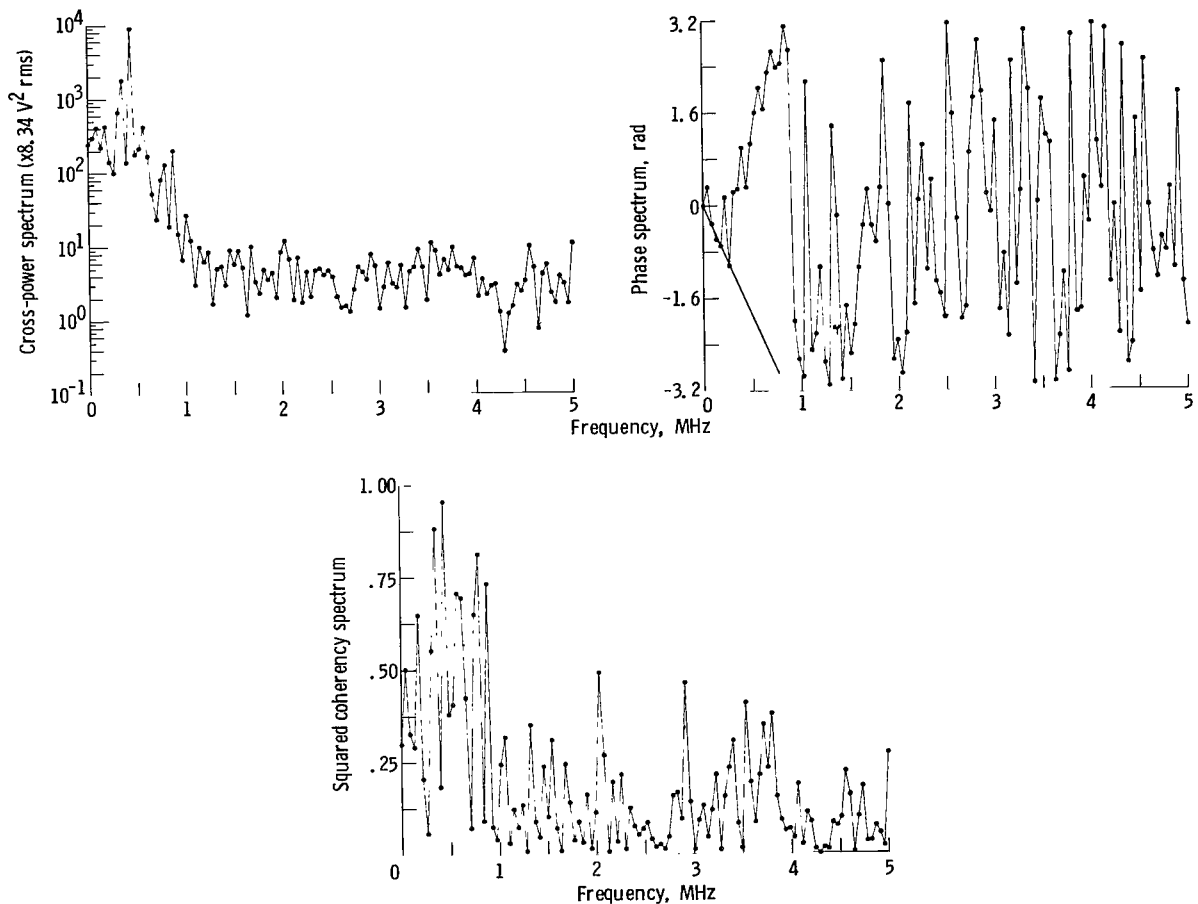


Figure 8. - Wave dispersion with electrodes 1 and 7 in plasma and 4-kilovolt anode voltage. Mode of operation, high pressure; sampling interval, Δt , 0.1 microsecond.

meters per second. The peaks at 352 and 572 kilohertz appear to be the sidebands of 440 kilohertz. The peaks at 792 and 1012 kilohertz appear to be the sidebands of the wave mode at 880 kilohertz. The pump that produces these sidebands is the wave mode at 88 kilohertz. The pump does get depleted. It appears only as a very weak peak in the cross spectrum. The peak with the maximum power in the whole spectral band in figure 8 is the peak at 440 kilohertz. Though the wave mode at 880 kilohertz is the second harmonic of the 440-kilohertz mode, the phase spectra at the corresponding frequencies suggest that the phase relation does not satisfy the resonance conditions. This is a case of nonresonant wave-wave interaction; that is, the resonance conditions for frequency are met ($2 \times 440 \text{ kHz} = 880 \text{ kHz}$), but the resonance conditions for the wave number (eq. (15)) are not satisfied. The wave at 440 kilohertz propagates with a velocity of 1.3×10^8 centimeters per second, and the wave at 880 kilohertz propagates with a velocity of 8.5×10^6 centimeters per second. That two measured velocities differ by a factor of 20 does not appear to be due to an experimental error or a computer software problem. The strong peaks at these frequencies in the cross-power spectrum are clearly associated with high values (>0.8) of coherency $|\gamma_{12}(\omega)|$. If an electron current is assumed to be flowing in the toroidal direction with the electrons at an electron kinetic temperature T_e of approximately 10 electron volts ($v_{the} = 1.88 \times 10^8$ cm/sec), the maximum wavelength of a perturbation will be approximately given by the major circumference of the torus, $2\pi R = 4.8$ meters, which translates to a disturbance of 394 kilohertz. Had the wavelength been limited to the minor circumference at the location of the probe, $2\pi r_p = 44$ centimeters, the frequency of a wave traveling at 1.88×10^8 centimeters per second would be 4.26 megahertz. It appears, however, that the wave mode at 880 kilohertz is due to an electron bunch, or spoke, propagating with the E/B drift velocity.

Low-Pressure (High Impedance) Mode

The low-pressure mode (LPM) of operation in the bumpy-torus experiment is characterized by an electron kinetic temperature T_e greater than 35 electron volts in deuterium and a neutral background density n_0 of less than 8.9×10^{11} particles per cubic centimeter ($<2.7 \times 10^{-5}$ torr, ref. 4). All the data presented in this section were taken (1) at a n_0 of 7.0×10^{11} particles per cubic centimeter (2.12×10^{-5} torr), (2) with electrodes 1 and 7 surrounding the plasma and all other electrodes withdrawn from the experimental plasma volume, and (3) with each electrode ring biased to a positive potential varying from 4 kilovolts to 14 kilovolts in 2-kilovolt steps. The ion kinetic temperature T_i was apparently so low that a useful charge-exchange neutral signal was not available even when 14 kilovolts was applied to the electrodes. The electron density as measured by the microwave interferometer varied from 3.4×10^8 to 5.8×10^8 electrons per cubic centimeter at 4 and 14 kilovolts, respectively, for the LPM.

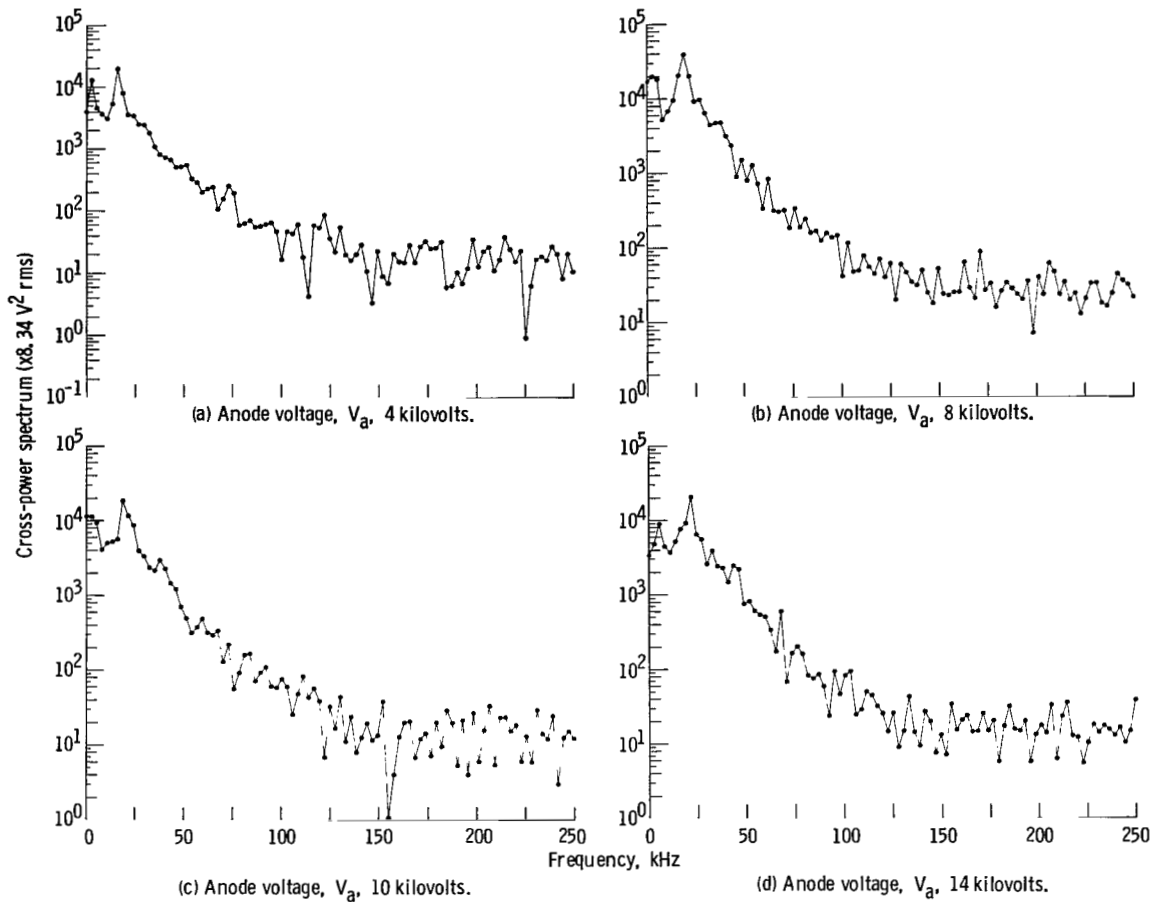


Figure 9. - Cross-amplitude spectra with electrodes 1 and 7 in plasma and anode voltages from 4 to 14 kilovolts. Mode of operation, low pressure; sampling interval, Δt , 2 microseconds.

Figure 9 shows the cross-power spectrum at anode voltages V_a of 4, 8, 10, and 14 kilovolts at constant B_{\max} and n_0 . The only peak at 4 kilovolts is at 16 kilohertz; the only peak at 8 kilovolts is at 19 kilohertz. The power spectrum decreases between the peak and 100 kilohertz. From 100 kilohertz to 250 kilohertz, the power level remains at about the same amplitude and corresponds to a fluctuation level of about 13 root-mean-square volts (V rms). At 10 kilovolts, in addition to the mode at 19 kilohertz, there appears to be a weak peak at the second harmonic of 19 kilohertz. Increasing V_a further to 14 kilovolts results in nonlinearity that causes the second and third harmonics to appear in addition to the fundamental oscillation at 22 kilohertz.

The change in the frequency of the fundamental wave mode from 4 to 14 kilovolts is very weakly dependent on the applied voltage. However, recall that in the high-pressure mode, with electrodes 1 and 7 in the plasma, the frequency of the dominant wave mode changed radically as the voltage was varied from 2 kilovolts to 4 kilovolts. Also, in figure 9 the strength of the fundamental-mode amplitude in the LPM remained at about

420 V rms even though V_a was varied from 4 kilovolts to 14 kilovolts. This suggests that the threshold for nonlinearity to begin is not a strong function of the wave amplitude. The threshold for harmonics to appear seems to be a V_a of 10 kilovolts. We have observed that the electron density curve changes slope as V_a goes above 10 kilovolts. A change in the slope of the voltage-current characteristic for the bumpy-torus discharge has also been reported (ref. 4) near 10 kilovolts in the LPM.

Figure 10 shows the cross-power spectrum, the phase spectrum, and the squared coherency spectrum for a V_a of 14 kilovolts. The peaks at 22, 44, and 66 kilohertz are related harmonically in frequency. The coherency spectrum indicates high $|\gamma_{12}(\omega)|$ at these frequencies. The fundamental mode propagates with an aximuthal phase velocity of 3.7×10^6 centimeters per second. A straight line drawn through the phase points corresponding to these frequencies and the origin reveals that all modes are propagating with the same phase velocity. The direction of propagation is the same as the E/B drift direction with the electric field pointing radially outward. The observed

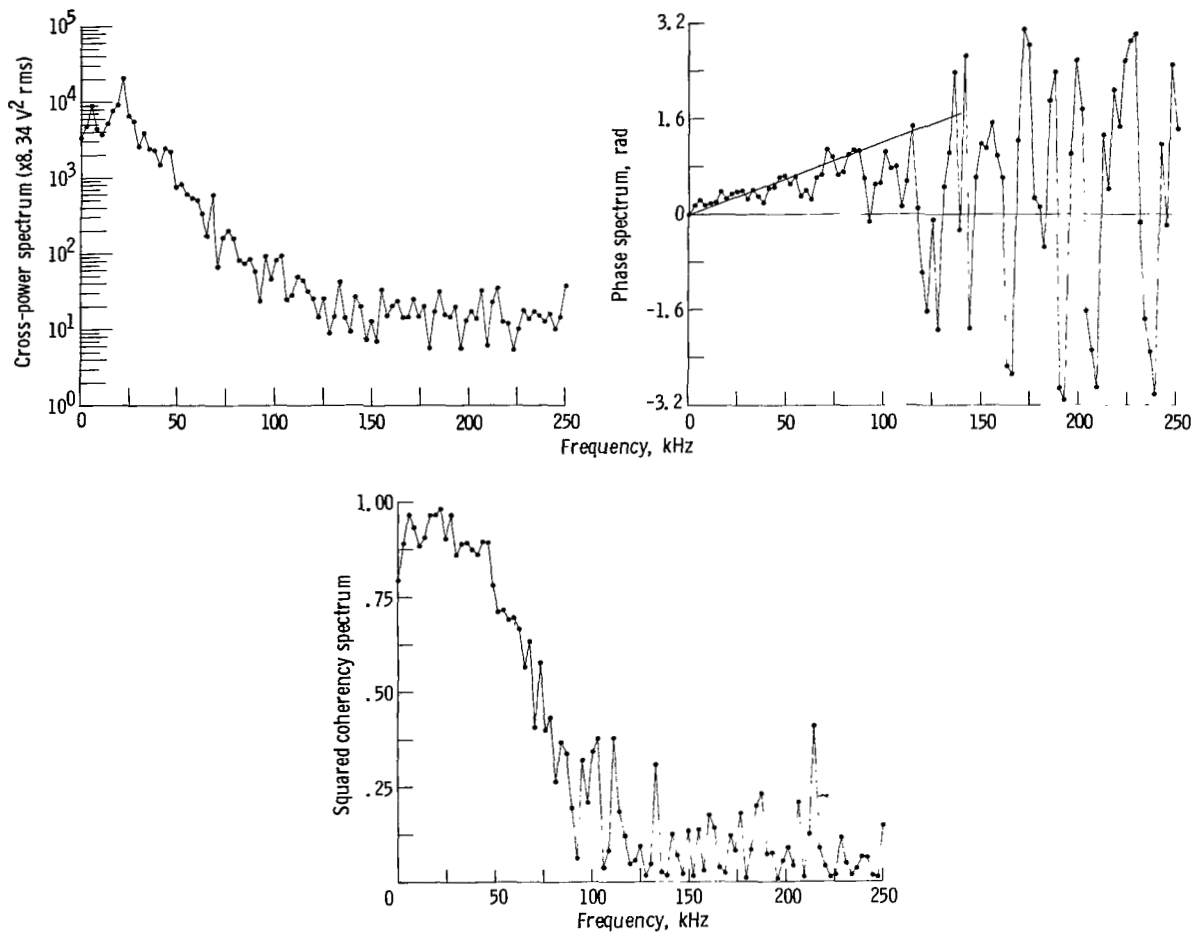


Figure 10. - Wave dispersion with electrodes 1 and 7 in plasma and 14-kilovolt anode voltage. Mode of operation, low pressure; sampling interval, Δt , 2 microseconds.

harmonic generation appears to be a resonant wave-wave interaction phenomenon in that the resonance conditions on both ω and k_θ are satisfied.

In figure 10 there are no peaks in the cross-power spectra from 75 to 250 kilohertz. In this frequency range the coherency $|\gamma_{12}(\omega)|$ is low (<0.6) and the phase spectrum is very jittery and random. This suggests that only noise or turbulence is present in this spectral band. Another feature of the phase spectra in all the experimental runs in the LPM, and represented in figure 10 for the run at 14 kilovolts, is that the phase spectrum exhibits hardly any jitter from very low frequencies to 75 kilohertz. This spectrum also exhibits very high coherency. Other than the few peaks already mentioned, the cross-power spectrum indicates a gentle decline in the power level in this spectral band. Because in this band the power levels are reasonable, the coherency is high, and the phase spectrum exhibits much less jitter, a continuum of coherent modes may be present in the plasma. The phase appears to be linearly related to the frequency. At first sight it appears that a disturbance propagating around a closed path or circle should have only discrete normal modes. However, as pointed out in the literature (refs. 13 to 15), two-dimensional shear flows and flows between rotating cylinders can give rise to a continuous spectrum of normal system modes. An experimental measurement of the azimuthal wave-phase velocity with radius should indicate whether our plasma better approximates the two-dimensional shear flow model or the rotating-cylinder model.

The plasma for the rotating-cylinder model can be visualized by assuming the central cylindrical core of the plasma to be one rotating cylinder and an electron sheath to be the other rotating cylinder. The electron sheath ($n_e > n_i$) can be physically located between the rotating plasma cylinder and the electrode ring. Previous investigations (refs. 2 to 4) have shown that rotating spokes of ions and electrons can exist simultaneously in this plasma.

Figure 11 presents the autopower spectrum rather than the cross-power spectrum for the same case as figure 10. The power and coherency spectra are presented for sampling intervals of 2 and 0.05 microsecond, respectively. There is noise in the 75-kilohertz-to-10-megahertz spectral band. This spectral band has very low coherency. The amplitudes of the fluctuations are only 2 volts rms in the spectral band from 1 to 10 megahertz.

Keeping B_{\max} and n_0 constant while raising V_a from 4 kilovolts to 14 kilovolts has shown (1) that the fundamental oscillation frequency remains approximately constant; (2) that the amplitude of this oscillation remains the same; (3) that the direction of propagation is the same as the E/B drift direction with the radial electric field pointing outward; (4) that the phase velocity in all cases is limited to 2×10^6 to 3×10^6 centimeters per second; (5) that almost all the power stored in the fluctuations lies in the spectral band 0 to 75 kilohertz; (6) that in addition to the discrete modes, a continuum of eigenmodes may exist at frequencies less than 75 kilohertz; and (7) that noise occupies the 75-kilohertz-to-10-megahertz frequency band.

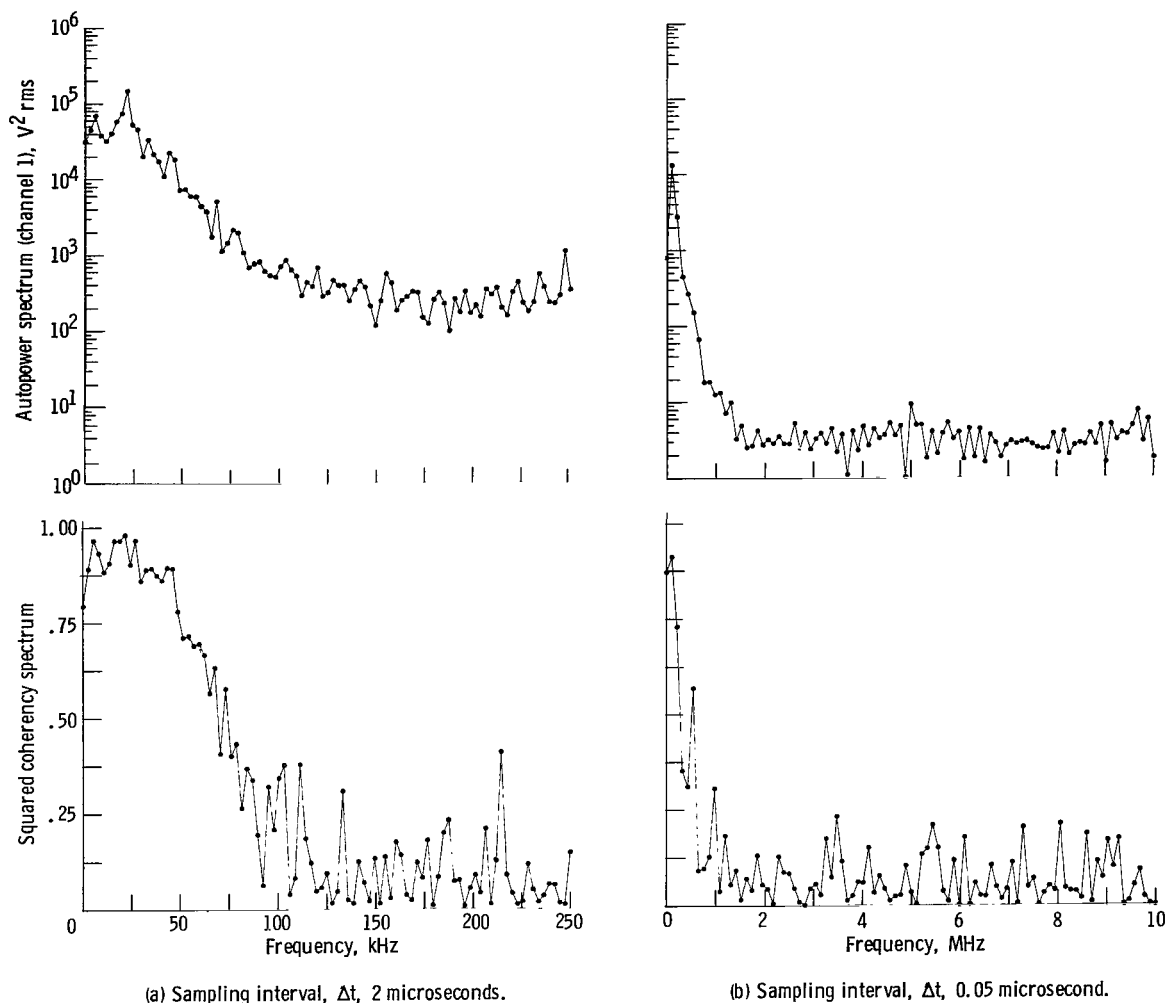


Figure 11. - Autopower spectra corresponding to figure 10.

What may be happening in the LPM as V_a is raised is that the potential drop or electric field in the sheath remains constant (so that E/B is constant) while the central plasma cylinder gets biased to higher and higher potentials as the voltage applied to the anodes is increased. An almost constant phase velocity is indicative of this. Also, if the primary driving force behind the instability originates in the sheath - for a constant E/B , the oscillation's frequency, amplitude, phase velocity, and direction of wave propagation would probably not change as the applied voltage is increased. The direction of the wave propagation agrees well with the E/B drift direction.